



Collective Behavior in a Granular Jet: Emergence of a Liquid with Zero Surface Tension

Xiang Cheng, German Varas,* Daniel Citron, Heinrich M. Jaeger, and Sidney R. Nagel

The James Franck Institute and Department of Physics, The University of Chicago, Chicago, Illinois 60637, USA

(Received 14 June 2007; published 1 November 2007)

We perform the analog to “water bell” experiments with granular jets. Rebounding from cylindrical targets, wide granular jets produce sheets or cones with shapes that mimic a zero-surface-tension liquid. The jets’ particulate nature appears when the number of particles in the cross section is decreased: the emerging structures broaden, gradually disintegrating into diffuse sprays. The experiment has a counterpart in the behavior of quark-gluon plasmas generated by colliding heavy ions. There, a high collision density gives rise to collective behavior also described as a liquid.

DOI: [10.1103/PhysRevLett.99.188001](https://doi.org/10.1103/PhysRevLett.99.188001)

PACS numbers: 45.70.Mg, 47.55.Ca

When one or two particles strike a smooth wall at normal incidence, they rebound in the direction whence they came. Yet, as we show here, a dense stream of non-cohesive particles hitting a target retains its integrity and deforms into a thin sheet with a shape resembling the structures created by an impinging water jet [1–4]. Thus, the collective behavior of many particles differs qualitatively from that of the individual components. When can a jet of discrete particles be modeled as a liquid [5–10], and how do the liquid patterns emerge out of individual particle scattering events from a target? Such questions, posed and investigated here with granular materials, have their counterpart in much more microscopic situations such as the quark-gluon plasma caused by high-energy collisions of gold ions at the Relativistic Heavy Ion Collider (RHIC), which also produces scattering patterns indicative of a liquid state [11]. Our findings provide a macroscopic, purely classical example of how strong interactions, mediated by rapid collisions in a densely packed region, can give rise to liquid behavior.

When a water stream hits a flat target, it spreads symmetrically in the direction transverse to the impact and deforms into a thin sheet. For targets smaller than the stream diameter, the sheet forms a hollow bell-shaped structure that envelopes the target. Such “water bells” were first reported in 1883 by Savart [1] and more recently studied systematically by Clanet [3]. By contrast, with the exception of several simulations and experiments on granular streams passing by solid obstacles at relatively low particle density and speed [12–14], little is known about the structures emerging from equivalent experiments using granular material. Here, we examine a noncohesive granular jet colliding with a target. For jets many particles wide, the impact produces granular sheets and cones similar to those seen for water with structures that depend on the ratio of the jet to the target diameter. In this regime, the granular medium behaves like a liquid with zero surface tension, which is appropriate for a system of noncohesive particles. The particulate nature of the material becomes apparent when the sheets and cones broaden and gradually disintegrate as the number of particles in the beam is decreased.

We prepared our dense jets by packing granular material into a 40 cm section of a glass launching tube of inner diameter $D_{\text{jet}} = 0.73$ cm [Fig. 1(a)]. The grains, which were compacted to a reproducible density by tapping, were monodisperse spherical beads of glass ($\rho = 2.5$ g/cm³, restitution coefficient 0.75 ± 0.05) or copper ($\rho = 8.2$ g/cm³) with diameters between $d = 50$ μm and $d = 2.1$ mm. Prior to filling the tube, we baked the beads

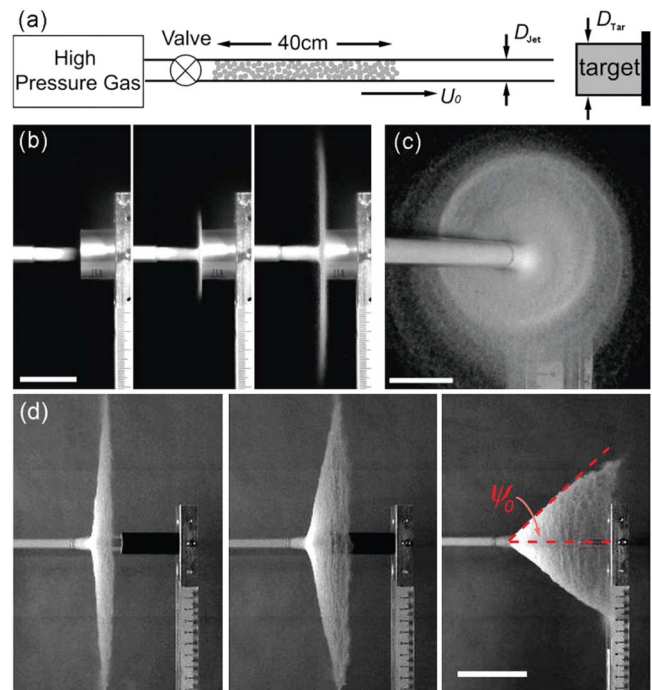


FIG. 1 (color online). Liquid-like granular sheets and cones. (a) Sketch of the experimental setup. (b) Side view of a granular jet comprised of 100 μm glass beads hitting a target at velocity $U_0 \sim 10$ m/s. The ratio of target-to-jet diameter is $D_{\text{Tar}}/D_{\text{Jet}} = 3.80$. The images show the jet 0.5 ms before as well as 2.5 and 9.5 ms after impact (left to right). Scale bar is 3.0 cm. (c) Axial view of the same granular sheet 35.5 ms after impact. Scale bar is 2.5 cm. (d) Side views of the hollow cones produced by 100 μm glass bead jets for smaller target-to-jet diameter ratios. $D_{\text{Tar}}/D_{\text{Jet}} = 2.0, 1.62,$ and 0.88 (left to right). Scale bar is 6.0 cm.

in vacuum to minimize any residual adhesion between beads. Pressurized gas accelerated this granular plug into a jet which hits a target 2.5 cm in front of, and collinear with, the tube. The jet velocity U_0 could be varied between 1 and 16 m/s. The impacts were filmed at 2000 frames/second. Figures 1(b) and 1(c) show the side and front views, respectively, of a colliding jet. Since there are few collisions inside it, the jet maintains its cylindrical shape before hitting the target, consistent with jets produced when a sphere impacts loosely packed powders [15,16]. After hitting the target, the jet deforms into an extraordinarily thin symmetric granular sheet clearly resembling a spreading liquid. To investigate the similarities between granular and liquid jets, we first keep the jet diameter, D_{Jet} , fixed at values much larger than the particle diameter, d , and vary the target diameter, D_{Tar} , as shown in Fig. 1(d). When D_{Tar} is reduced, the sheets change into cones with opening angle $\psi_0 < 90^\circ$. Figure 2 shows that ψ_0 increases linearly with $D_{\text{Tar}}/D_{\text{Jet}}$ until ψ_0 saturates at 90° above $D_{\text{Tar}}/D_{\text{Jet}} \sim 2$. Glass and copper beads produce essentially identical behavior.

We can compare our results with those from Clanet [3] for water jets, who found that the opening angle, ψ , of the “water bell” depends on the Weber number $We = \rho U_0^2 D_{\text{Jet}} / \sigma$, where U_0 is the jet velocity and ρ the density and σ the surface tension of water. In the large-We limit (large U_0 or small σ), ψ approaches a constant, ψ_0 , that depends only on $D_{\text{Tar}}/D_{\text{Jet}}$. Figure 2 shows excellent overlap of our values for ψ_0 with those of Clanet. As shown in the inset to Fig. 2, ψ for granular material remains constant

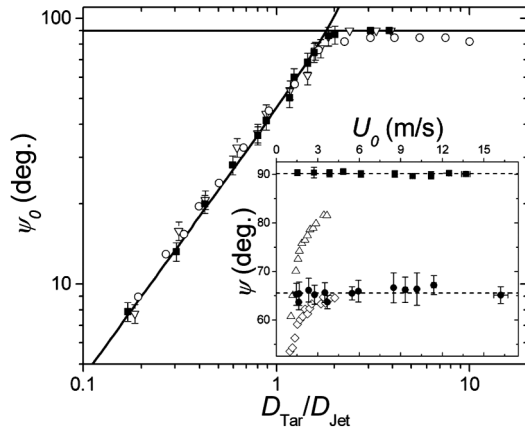


FIG. 2. Opening angle of the granular sheets and cones. Angle ψ_0 as a function of $D_{\text{Tar}}/D_{\text{Jet}}$ for 100 μm glass beads (\blacksquare), 100 μm copper beads (∇), and water in the large-We limit (\circ). The only observable difference is that ψ_0 at large $D_{\text{Tar}}/D_{\text{Jet}}$ is $\sim 85^\circ$ for water but 90° for grains. The solid lines are fits of Eq. (1) with $(A - B) = 0.30$ for $D_{\text{Tar}}/D_{\text{Jet}} < 2$. Inset: Angle ψ as a function of jet velocity U_0 for 100 μm glass beads with $D_{\text{Tar}}/D_{\text{Jet}} = 2.47$ (\blacksquare) and $D_{\text{Tar}}/D_{\text{Jet}} = 1.32$ (\bullet), and for water with $D_{\text{Tar}}/D_{\text{Jet}} = 3.29$ (\triangle) and $D_{\text{Tar}}/D_{\text{Jet}} = 1.33$ (\diamond). The horizontal lines are $\psi = 90^\circ$ (top) and $\psi = 65.5^\circ$ (bottom). Data for the water are taken from [3].

as U_0 is varied over our entire experimental range (an order of magnitude) whereas ψ for water decreases at small velocities. This suggests a granular jet impacting as the target behaves like a liquid with negligible surface-tension: regardless of the value of U_0 , the Weber number is pinned at infinity since the absence of significant cohesive forces effectively drives the surface tension to zero. With a cohesive granular material, we found that ψ is smaller than that of noncohesive granular material at the same U_0 .

The linear dependence of ψ_0 on $D_{\text{Tar}}/D_{\text{Jet}}$ in the large-We limit can be understood from momentum conservation. The magnitude of the momentum of the incoming granular jet reaching the target in time τ is $P_{\text{in}} = (\pi/4)\rho D_{\text{Jet}}^2 U_0^2 \tau$. The collisions of the jet with the target are inelastic so the outgoing momentum magnitude $P_{\text{out}} = CP_{\text{in}}$ where C is the average coefficient of restitution. Along the axis, the momentum balance is given by: $P_{\text{in}} - P_{\text{out}} \cos\psi_0 = P_{\text{in}}(1 - C \cos\psi_0) = F_{\text{Tar}}\tau$, where F_{Tar} is the average force along the axis exerted by the target on the jet. Transverse to the axis, the momentum (averaged over the entire sheet) remains zero. When $D_{\text{Tar}}/D_{\text{Jet}} < 1$, $F_{\text{Tar}} = (A\pi/4)D_{\text{Tar}}^2 \rho U_0^2$. Here, A is a constant describing the average glancing collision angle for a particle. In this region, the average restitution coefficient, C , also depends on the fraction of particles hitting the target: $C = [1 - B(D_{\text{Tar}}/D_{\text{Jet}})^2]$ where B depends on the coefficient of restitution for single collisions. When $D_{\text{Tar}}/D_{\text{Jet}} \gg 1$, the entire momentum of the jet is reflected by the target. Finally, we obtain

$$\psi_0 = \begin{cases} \arccos[1 - (A - B)(\frac{D_{\text{Tar}}}{D_{\text{Jet}}})^2]; & \frac{D_{\text{Tar}}}{D_{\text{Jet}}} \ll 1 \\ 90^\circ; & \frac{D_{\text{Tar}}}{D_{\text{Jet}}} \gg 1 \end{cases} \quad (1)$$

Clanet reached the same result by considering the momentum transfer during the impact of a water jet on a target using hydrodynamic equations [3]. By fitting the experimental data in Fig. 2, we find $(A - B) = 0.30 \pm 0.02$ which is close to the value ≈ 0.352 for water [3].

The impact of dense particle streams clearly generates similar patterns as do liquids. How does the particulate nature of granular material becomes manifest as the number of particles within the jet decreases? To vary this number, we change the ratio, D_{Jet}/d , of jet to particle diameter. In the limit $D_{\text{Tar}}/D_{\text{Jet}} \gg 1$, Figs. 3(a)–3(c) show major qualitative changes in the particle trajectories as D_{Jet}/d is reduced. The images were created by superimposition of many different consecutive still images; each pixel shows the maximum intensity at that location over all images in the time period. For $D_{\text{Jet}}/d = 73$, almost all particles emerge in a sheet normal to the jet axis. For $D_{\text{Jet}}/d = 14.6$, the sheet becomes more diffuse as some particles leave the plane as shown by the bright lines. For $D_{\text{Jet}}/d = 3.5$, a firework-like pattern results after impact and sheet structure is no longer apparent as particles rebound from the target in a broad angular distribution. To quantify this trend, we plot in Fig. 3(d) the angular scat-

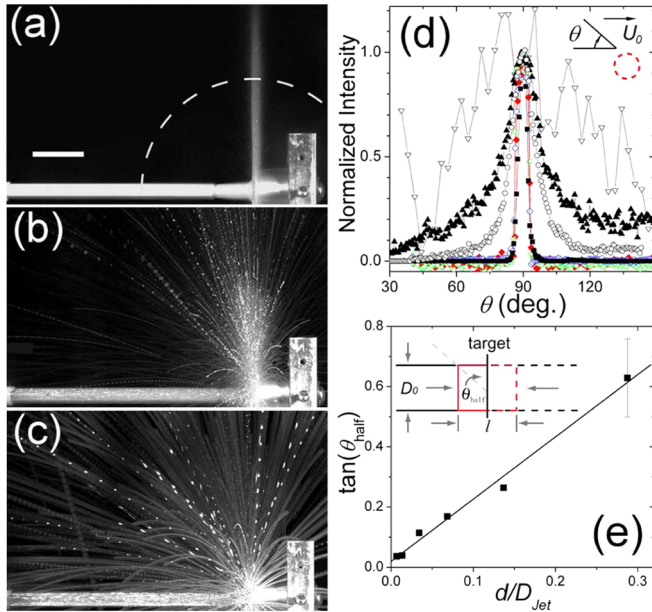


FIG. 3 (color online). Scattering patterns as a function of particle density across the jet diameter. (a)–(c) Side view of the same geometry as shown in Fig. 1(a). Maximum intensity projections of the scattering process for fixed $D_{\text{Tar}}/D_{\text{Jet}} = 3.8$ but varying particle density: (a) $D_{\text{Jet}}/d = 73$; (b) $D_{\text{Jet}}/d = 14.6$; (c) $D_{\text{Jet}}/d = 3.5$. (d) Normalized scattering profiles for glass beads in air with $D_{\text{Jet}}/d = 73$ (■), $D_{\text{Jet}}/d = 29.2$ (○), $D_{\text{Jet}}/d = 14.6$ (▲), $D_{\text{Jet}}/d = 3.5$ (▽); glass beads in helium $D_{\text{Jet}}/d = 73$ (◆); copper beads in air $D_{\text{Jet}}/d = 73$ (◁), and rough sand in air $D_{\text{Jet}}/d = 73$ (◇). The arrow and the dashed circle in the inset indicate the direction and the cross section of the jet. (e) Half-width θ_{half} of the angular scattering profiles in (d) as a function of d/D_{Jet} . Solid line is a linear fitting. The model is sketched in the inset and explained in the text.

tering distribution, obtained by averaging images as in Figs. 3(a)–3(c) along a circle of radius $r = 8.7D_{\text{Jet}}$ centered on the jet axis [shown partially in Fig. 3(a) as the dashed line]. The axial position of the center is chosen to be in the middle of the ejected particles, which gradually moves away from the target as the particle diameter d increases. To avoid the target holder, only the profile along the upper half of the circle is plotted. Each profile is normalized to its peak value. The scattering angle θ is zero along the axis of the jet and increases clockwise. As D_{Jet}/d decreases, these profiles broaden.

To investigate this crossover to diffuse scattering, we examined the roles of air and inelasticity during interparticle collisions. To exclude air as the primary cause of the sheet formation, three experiments were performed. (i) Doing the entire experiment in a helium atmosphere and using helium as the accelerating gas, which reduces the density and kinematic viscosity of the gas, produced no change in the angular distribution, as shown in Fig. 3(d) for $D_{\text{Jet}}/d = 73$. (ii) Performing our experiment at reduced ambient pressure of 31 Pa also resulted in a thin, planar

sheet structure. (31 Pa corresponds to a mean free path of air molecules that is 3 times the $100 \mu\text{m}$ grain diameter used in Fig. 3(a). Although air at atmospheric pressure accelerates the granular column from behind, we estimate that the velocity of air penetrating into a 40 cm granular pack comprised of $100 \mu\text{m}$ beads with packing fraction around 0.6 is 2 orders of magnitude smaller than the velocity of the jet. Thus, by the time the front of the jet hits the target, a negligible amount of air has entered the chamber.) (iii) We decreased the tube diameter D_{Jet} , but fixed the particle-air interaction by keeping $d = 100 \mu\text{m}$. In this case, the planar structure shown in Fig. 3(a) disappeared gradually, and for $D_{\text{Jet}} \sim d$, we regained the firework pattern shown in Fig. 3(c). In addition, we altered the interparticle collision dynamics by changing the particle material or the surface roughness. Figure 3(d) shows that for copper particles that are less elastic than glass or for rough sand particles, the angular scattering distribution remains unchanged. However, distributions for the same D_{Jet}/d do not overlap quantitatively for different d , and the liquidlike sheets tend to be more sharply delineated with smaller particles.

While we cannot rule out that inelastic collisions or effects of air affect the detailed shape of the scattering profiles, our results imply that the creation of the sheets arises fundamentally from the rapid collisions occurring in an interaction region right in front of the target. We found similar behavior when two granular jets collide head-on, implying that the target serves primarily to reverse the direction of particles incident upon it. For this situation, a simple geometric model can capture the essence of the crossover from fluid to granular behavior. As shown in Fig. 3(e), inset, we divide the system into three zones: two external regions in which the jets are traveling towards one another but have not yet collided, and an interaction region with the same diameter as the jets, D_{Jet} , and axial length, l . Inside the interaction region particles undergo rapid collisions and are confined by pressure from the incoming jets on both sides. The only way in which particles can escape (which they must since new particles are entering the region continuously) is to emerge perpendicularly to the jet axis. A measure for deviations from this transverse axis and thus for the half-width of the angular distributions in Fig. 3(d) is the angle θ_{half} by which particles can escape ballistically from the center of the beam. By geometry, this is given by $\tan(\theta_{\text{half}}) = l/(D_{\text{Jet}})$. For dense particle streams where the mean free path is much smaller than the diameter of the particles, we expect $l \sim 2d$ since that is the smallest region occupied by the two colliding particles. Therefore, the half-width should scale as $\theta_{\text{half}} = \arctan(\alpha 2d/D_{\text{Jet}})$ where α is a constant $O(1)$. This dependence on particle density d/D_{Jet} across the beam is indeed born out by the data in Fig. 3(e), with $\alpha = 1.05 \pm 0.05$. As a result, when D_{Jet}/d is sufficiently large, the majority of particles undergo rapid, multiple collisions in front of the target and are ejected into a narrow angle,

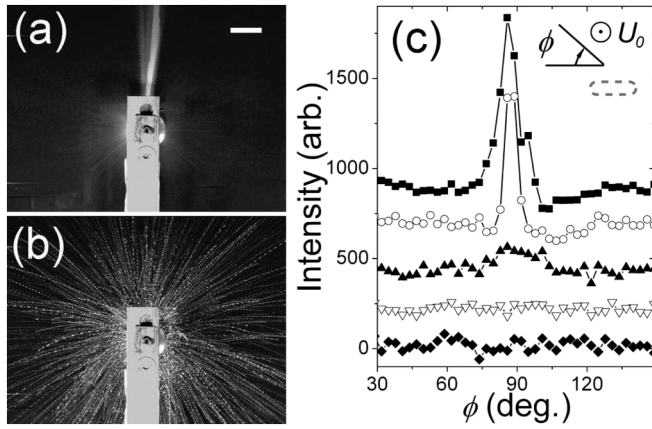


FIG. 4. Azimuthal scattering profiles for granular jets with rectangular cross section (aspect ratio 2). Shown are views along the axial direction, looking at the target from behind. (a) Anisotropic profile resulting for $D_{\text{Jet}}/d = 73$, where D_{Jet} is the long axis of the jet cross section. The target holder blocks the view of the scattered portion shooting downward. Scale bar is 3.0 cm. (b) Isotropic profile resulting for $D_{\text{Jet}}/d = 7$. (c) Azimuthal profiles along a circle with $r = 8.7D_{\text{Jet}}$ for $D_{\text{Jet}}/d = 73$ (\blacksquare), $D_{\text{Jet}}/d = 29.2$ (\circ), $D_{\text{Jet}}/d = 14.6$ (\blacktriangle), $D_{\text{Jet}}/d = 7$ (∇), and $D_{\text{Jet}}/d = 3.5$ (\blacklozenge). The direction and the cross section of jet are shown in the inset; ϕ is taken to be zero along the long axis of the jet cross section.

similar to a liquid film. For example, $\theta_{\text{half}} < 2^\circ$ for jets with $D_{\text{Jet}}/d > 60$.

When the granular scattering mimics that of a liquid, we expect azimuthally anisotropic patterns to be created by jets with rectangular cross sections. The incoming jets establish an elongated interaction region within the plane transverse to the beam (azimuthal ϕ -direction) so that more particles will escape along the short axis of the cross section. This is also the situation pertinent to noncentral collisions of heavy ions at RHIC where partial overlap of the colliding ions establishes an elongated interaction zone for the quark-gluon plasma. Azimuthally anisotropic scattering patterns have been taken as the main evidence for liquidlike behavior of this plasma [11]. As shown in Fig. 4(a) for $D_{\text{Jet}}/d \gg 1$, we observe sharply focused azimuthal patterns for granular jets with rectangular cross section. To quantify the anisotropy and compare with the RHIC results [11], we analyze the second coefficient, v_2 , of the Fourier expansion of the azimuthal scattering profiles in Fig. 4(c). For $D_{\text{Jet}}/d = 73$, $v_2 = 0.16$. Normalizing v_2 by the parameter of spatial anisotropy $\epsilon_x = (c^2 - 1)/(c^2 + 1)$ (c is the aspect ratio of the collision area) to remove the trivial geometrical effect, we have $v_2/\epsilon_x = 0.26$ larger than the typical value (0.24) at

RHIC [17]. As Figs. 4(b) and 4(c) show, the scattering patterns become more isotropic with decreasing D_{Jet}/d .

These experiments demonstrate how noncohesive granular material can produce collective motion reminiscent of liquids. Our results suggest that rapid particle collisions in a very narrow interaction region, with thickness of a few particle diameters, eject very thin granular sheets that mimic the liquids without surface tension. The crossover between diffuse and sharp scattering profiles appears to be controlled primarily by the number of collisions in the jet. These findings may have analogs in other, disparate parts of physics, where a high density of collisions dominates the behavior.

We thank R. Bellwied, E. Corwin, S. Gavin, T. Pöschel, J. Royer, T. Witten, and L. Xu. This work was supported by the NSF through its MRSEC program under No. DMR-0213745 and under No. DMR-0303072, and by the W. M. Keck Foundation.

*Present address: Departamento de Física, Universidad de Chile, Casilla 487-3, Santiago, Chile.

- [1] F. Savart, Ann. Chim. (Paris) **54**, 56 (1833); **54**, 113 (1833).
- [2] G. I. Taylor, Proc. R. Soc. A **253**, 289 (1959).
- [3] C. Clanet, J. Fluid Mech. **430**, 111 (2001).
- [4] J. M. Aristoff, C. Lieberman, E. Chan, and J. W. M. Bush, Phys. Fluids **18**, 091109 (2006).
- [5] L. P. Kadanoff, Rev. Mod. Phys. **71**, 435 (1999).
- [6] I. S. Aranson and L. S. Tsimring, Rev. Mod. Phys. **78**, 641 (2006).
- [7] H. M. Jaeger, S. R. Nagel, and R. P. Behringer, Rev. Mod. Phys. **68**, 1259 (1996).
- [8] P. Jop, Y. Forterre, and O. Pouliquen, Nature (London) **441**, 727 (2006).
- [9] S. T. Thoroddsen and A. Q. Shen, Phys. Fluids **13**, 4 (2001).
- [10] F. Melo, P. Umbanhowar, and H. L. Swinney, Phys. Rev. Lett. **72**, 172 (1994).
- [11] I. Arsene *et al.* (BRAHMS Collaboration), Nucl. Phys. A **757**, 1 (2005); B. B. Back *et al.* (PHOBOS Collaboration), *ibid.* **757**, 28 (2005); J. Adams *et al.* (STAR Collaboration), *ibid.* **757**, 102 (2005); K. Adcox *et al.* (PHENIX Collaboration), *ibid.* **757**, 184 (2005).
- [12] V. Buchholtz and T. Pöschel, Granular Matter **1**, 33 (1998).
- [13] Y. Amarouchene, J. F. Boudet, and H. Kellay, Phys. Rev. Lett. **86**, 4286 (2001); Phys. Fluids **18**, 031707 (2006).
- [14] E. C. Rericha, C. Bizon, M. D. Shattuck, and H. L. Swinney, Phys. Rev. Lett. **88**, 014302 (2001).
- [15] D. Lohse *et al.*, Phys. Rev. Lett. **93**, 198003 (2004).
- [16] J. Royer *et al.*, Nature Phys. **1**, 164 (2005).
- [17] P. F. Kolb, J. Sollfrank, and U. Heinz, Phys. Rev. C **62**, 054909 (2000).